Lifetime measurement of the Ar XIV $1s^2 2s^2 2p\ ^2P^o_{3/2}$ metastable level at the Heidelberg electron-beam ion trap

A. Lapierre,* J. R. Crespo López-Urrutia, J. Braun, G. Brenner, H. Bruhns, D. Fischer, A. J. González Martínez, V. Mironov, C. Osborne, G. Sikler, R. Soria Orts, H. Tawara, and J. Ullrich
Max-Planck Institut für Kernphysik, Saupfercheckweg 1, D-69117 Heidelberg, Germany

V. M. Shabaev, I. I. Tupitsyn, and A. Volotka
Department of Physics, St. Petersburg State University, Oulianovskaya 1, Petrodvorets, 198504 St. Petersburg, Russia
(Received 18 February 2006; published 22 May 2006)

We present the details of an accurate lifetime measurement of the $1s^2 2s^2 2p\ ^2P^o_{3/2}$ metastable level in boronlike Ar XIV performed at the Heidelberg electron beam ion trap [A. Lapierre *et al.*, Phys. Rev. Lett. **95**, 183001 (2005)]. The lifetime was inferred from decay curves resulting from deexcitation of the metastable level to its $^2P^o_{1/2}$ ground state through a magnetic-dipole ($M1$) transition upon cyclically turning on and off the electron beam. The measured lifetime of $9.573(4)(^{+12}_{-5})$ ms (stat)(syst) is in disagreement with a trend of theoretical predictions of 9.53(1) ms, which include the effect of the electron anomalous magnetic moment. Systematic effects were investigated by studying with high statistical significance the dependence of the decay times of the curves on various trapping conditions. The asymptotic trend of the decay times observed for increasingly high trapping potentials, which indicates negligible ion losses within a ms time scale, is in agreement with a theoretical model describing the ion escape rate in electrostatic ion traps. However, for high trapping potentials, we observed an unexpected slowly decaying component suggesting the presence of trapped low-energy electrons. Their origin, dynamics, and temperature, as well as their possible effects on the measured lifetime were investigated.

DOI: 10.1103/PhysRevA.73.052507 PACS number(s): 32.70.Cs

I. INTRODUCTION

For several decades, accurate measurements of atomic transition energies and excited-state lifetimes in highly charged ions (HCIs) have been an active field of considerable interest in atomic physics. In HCIs, relativistic, nuclear-structure and quantum electrodynamic (QED) effects scale with high powers of the effective nuclear charge $Z_i=Z-N+1$ (nuclear charge number Z and electron number N) and at the same time their electronic structure becomes simpler as the number of bound electrons is reduced. Hence they represent ideal systems to test and benchmark such contributions in atomic-structure theory.

Measurements related to fine-structure energy levels forbidden to decay via the electric-dipole ($E1$) interaction are of particular importance to develop relativistic and QED theories in medium and strong electromagnetic fields. The transition energies between levels of a same LS term (fine-structure splitting) can be highly sensitive to such contributions because, essentially, these levels are relativistic in origin and their energy separations can be small in comparison to QED effects. For instance, over the last few years, *ab initio* atomic-structure calculations in the framework of QED have become increasingly accurate, and QED contributions to the energy of the forbidden transition $1s^2 2s^2 2p\ ^2P^o_{1/2}$-$^2P^o_{3/2}$ of the boronlike Ar XIV ground state configuration have been found to be as large as 0.2% [1], while those to the lifetime of the Ar XIV $2p\ ^2P^o_{3/2}$ metastable level were found to be more than 0.5% [2].

Measurements of the energy of this particular forbidden transition, which can be observed in the solar corona, have recently been performed with an accuracy level of around 0.3 parts-per-million (ppm) [3,4]. The three recent lifetime measurements of this metastable level [5–7] have an accuracy level of about 2% which does not yet allow one to distinguish between theoretical models. Accurate lifetime measurements are essential since they reveal the transition line strength for the different multipole interactions. This information is complementary to that contained in the transition energies and thus other aspects of atomic theory can be tested by providing nonaveraged information on the amplitude of the expansion coefficients in an individual basis of the electronic wave function. Therefore high-precision measurements exposing relativistic as well as QED effects in the lifetime of this metastable level certainly deserve experimental investigations.

Here we present experimental details of a lifetime measurement of the boronlike Ar XIV $1s^2 2s^2 2p\ ^2P^o_{3/2}$ level at the electron beam ion trap of the Max-Planck-Institut für Kernphysik in Heidelberg (HD-EBIT) [8] performed by monitoring the temporal decay of optical fluorescence from the magnetic-dipole ($M1$) $2p\ ^2P^o_{1/2}$-$^2P^o_{3/2}$ transition [$\lambda=441.2559(1)$ nm in air [3]]. The high statistical significance achieved in the decay curve measurements allowed us to efficiently understand the temporal evolution of the population of trapped ions under observation by studying its sensitivity to the trapping potential and other trap parameters (electron beam current and energy, neutral density). As a consequence, we reached an accuracy level of 0.1%, which is $\approx$5 times smaller than the calculated contribution of the electron anomalous magnetic moment (EAMM) to the life-

*Present address: Department of Physics, University of California at Berkeley, Berkeley, California 94720, USA.

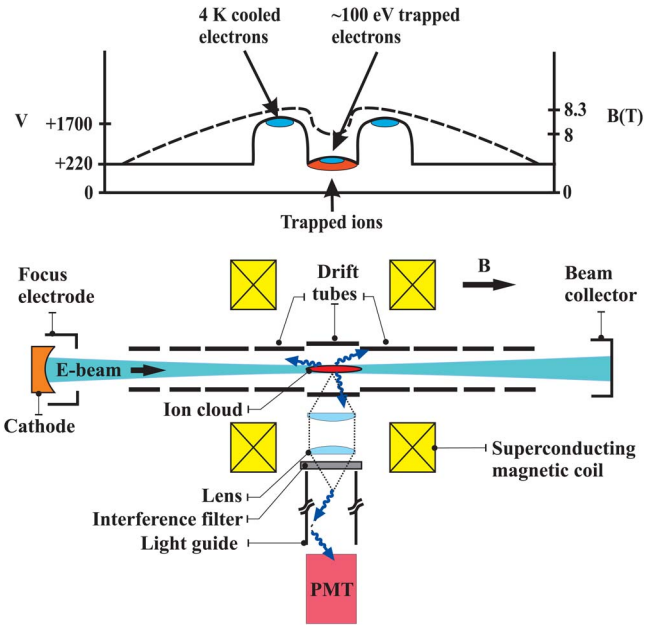

FIG. 1. (Color online) Schematic drawing of the experimental setup. In the upper diagram, the magnetic field flux density along the electron beam propagation direction is represented by a dashed line while the solid line represents the electrostatic trapping potential in the axial direction, only. Ions are trapped in the radial direction by the electron beam space charge potential (ESCP) and the magnetic field ($\mathbf{v}\times\mathbf{B}$ Lorentz force). The trap length was 40 mm.

time of this metastable level [2]. This paper is divided as follows: Section II presents the experimental method which includes details of the Heidelberg EBIT and the experimental procedure. Section III presents the data analysis procedure and investigates several systematic effects. Section IV investigates the origin of the slowly decaying background component and shows that this background might be caused by trapped electrons. Finally, before concluding, Sec. V confronts our experimental result to various theoretical predictions and shows the theoretical treatment used to include the EAMM effect to the lifetime of metastable levels.

II. EXPERIMENTAL METHOD

A. Electron beam ion trap: EBIT

EBITs produce and confine HCIs. In an EBIT (see Fig. 1), electrons are produced by a thermionic cathode of a Pierce-geometry electron gun biased to a negative potential, focused by a focus electrode, and extracted by an anode biased to a positive potential. Then, the electrons are accelerated up to keV energies towards a series of drift tubes at the trap center by a potential difference between the cathode and the drift tube assembly. Towards the trap center the electron beam is compressed by a strong magnetic field of 8 T (see dashed line in the upper part of Fig. 1) generated by two superconducting coils in a Helmholtz configuration, reaching a current density of more than 10^4 A/cm^2 and a beam diameter of less than 100 μm. This high flux of monoenergetic electrons causes efficient ionization of the atoms crossing the beam. The resulting ions are then trapped radially by the electron beam space charge potential (ESCP) as well as by the magnetic field, and also axially by appropriate electrostatic potentials applied to the drift tubes. The trapped ions are then sequentially brought to very high charge states by continuous electron-impact ionization. The electron beam is decelerated after passing the trap and dumped in a water-cooled electron collector. Due to the cryogenic environment (the central parts of the apparatus are cooled to 4 K) and the efficient differential pumping provided by thermal shields at 40 and 16 K, respectively, the neutral gas density at the trap center is extremely low (less than 10^{-12} mbar). The use of a differentially pumped chamber (called gas injector) producing an atomic beam directed towards the trap center enables one to change that value within certain limits.

B. Optical imaging and detection systems

In an EBIT, radiation (x ray, UV, or visible light) produced by excitation of the trapped ions by the electron beam can be observed through viewports. For the present lifetime measurement at the HD-EBIT, we used the viewport devoted to optical spectroscopy [3,9] equipped with two $f/4$ quartz lenses ($\oslash$38 mm, $f=150$ mm) located inside the EBIT vacuum to collect photons. This setup allowed us to image the cigar-shaped ion cloud in its entirety on a charge coupled device (CCD) camera outside of the vacuum chamber. Its measured length was slightly less than the nominal trap length of 40 mm [distance between drift tubes (DT) #4 and #5] and its diameter was smaller than 1 mm.

In order to efficiently guide light from the trap to a Peltier-cooled photomultipler tube (PMT) located far from the EBIT magnetic field, a 1150-mm long pipe made of a 50-mm inner-diameter aluminum tube was used whose interior was mechanically polished for optimum reflectivity. Prior to entering this light guide, photons of the wavelength of interest were selected by an interference filter with a 60% transmission and a 3-nm bandwidth [full width at half maximum (FWHM)] at 442 nm ($\sim 5°$ acceptance angle). With this filter we ensured that only the spectral line under investigation was observed and lines which could have possibly originated from impurity ions (e.g., C, N, O, Ba, W) or argon ions in other charge states were excluded. The most important task of the filter, however, was to reduce the glow of the thermionic cathode.

Our data acquisition and detection system is shown in Fig. 2. The signal pulses produced by the PMT were sent to a preamplifier, processed by a discriminator and a coincidence unit, and registered with one of the counters of a general purpose CAMAC event mode data acquisition system (DAQS). For the time calibration, a second counter registered pulses generated by a quartz-stabilized digital delay/pulse generator running at 20 or 9 kHz, respectively (first or second series of measurements). The average dead time (t_{dead}) of the PMT, preamplifier, discriminator, and coincidence unit ensemble was measured to be 1.4(1) μs.

C. Experimental procedure

The lifetime of the Ar XIV $2p\ ^2P^o_{1/2}$ metastable level was measured by observing optical decay curves resulting from

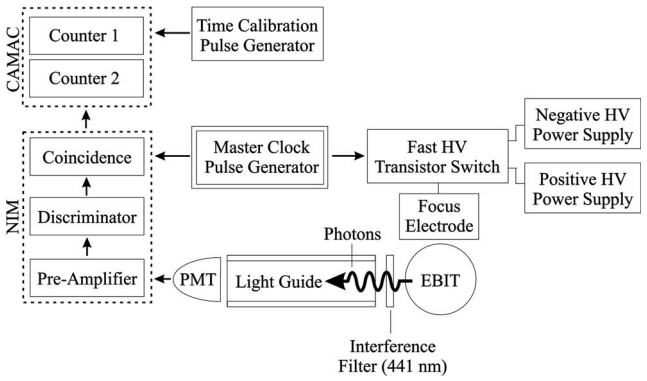

FIG. 2. Schematic drawing of the data acquisition and detection systems used for the lifetime measurement.

its deexcitation to the $2p\ ^2P^o_{1/2}$ ground "state" (level) in the so-called magnetic trapping mode [10–16]. This was realized by cyclically turning on and off the electron beam (i.e., alternating excitation and free decay). For this purpose, positive and negative high voltage (HV) was accordingly applied to the focus electrode of the electron gun by using a fast HV transistor switch having a rise time of a few ns, although the current limitations of the power supplies used lengthened its response time. A turn-off time of the electron beam of less than 500 μs was measured with a digital oscilloscope (see the following sections for investigations of systematic effects related to the turn-off time).

The arrival time of the photons was measured in relation to the pulse produced by a digital delay/pulse generator used as a master clock, which, at the same time, also triggered the HV transistor switch to turn the electron beam off (see Fig. 2). The data acquisition gate used for that purpose started 10 ms before the electron beam was turned off and stopped 15 ms after it was turned on once again.

In a first series of measurements, the EBIT was operated at a magnetic field flux density of 8 T. The voltage applied to the thermionic electron emitting cathode was −800 V and the drift tube assembly was biased to 220 V. The electron beam current was typically set to 100 mA (also to 50 and 60 mA for two run times). By using the procedure described in Sec. IV B 2, the combined and total space charge potential (TSCP) of the electron beam (ESCP) and the ion cloud (ISCP) was found to be approximately equal to $\Phi_T = -0.0028I/\sqrt{E_{eff}}$, where I is the electron beam current in mA and E_{eff} is the electron beam energy in keV. The prefactor was determined by keeping the trapping drift tubes at a high potential and, hence, this energy correction took into account the effect of a potential gradient between the trapping drift tubes and the central drift tube. Using this relation, the actual interacting electron beam energy was estimated to be $\cong$697 eV at the center of the trap, which was then sufficient to ionize Ar XIII but not Ar XIV, their respective ionization potentials being 686 and 755 eV [17]. The electron beam was turned off for 200 ms and on for 483 ms by applying −1300 and 1000 V to the focus electrode, respectively, resulting in a data acquisition time of 225 ms at a repetition rate of 1.464 s^{-1} (cycle period of 683 ms). The PMT dark count rate was measured to be 34 s^{-1} at a bias voltage of −1500 V. The PMT dark count rate was obtained from independent measurements taken by switching on and off the focus electrode while keeping the electron emission off. The uniform backgrounds obtained from these measurements were in agreement with others taken as the emission was on but the gas injection off as well as with backgrounds obtained with no drift tube trapping potentials when the electron emission was on, the electron beam was switched off, and the gas injection on.

In a second series of measurements, the electron gun was realigned by moving it in the radial direction to minimize the suppressor current. The suppressor is a ring-shaped electrode with an 16 mm diameter aperture located in front of the collector electrode. Its purpose is to repel secondary electrons liberated on the inner surface of the collector by the electron beam dumped on it. The suppressor current is due to beam electrons deviating from the central trajectory, and is a very good indicator of the proper tuning of the electron beam parameters. Its value is typically of a few μA. The drift tube assembly was biased to 200 V and the electron beam current was fixed at 90 mA because at 100 mA we observed a stronger slow component due to what we believe to be instabilities in the electron beam. For this setup, the electron beam energy was $\cong$715 eV. The electron beam was turned off for 1 s and on for 700 ms by respectively applying −1800 and 1000 V to the focus electrode resulting in data taking for 1025 ms at a rate of 0.588 s^{-1} (cycle period of 1700 ms). The dark count rate of the PMT, which was then biased to −1250 V, was 30 s^{-1}.

For both series, an argon atomic beam was ballistically injected into the EBIT from a differentially pumped injector chamber, which had a pressure of 10^{-8} mbar already at its first stage. The pressure measured outside the 40 K thermal shield of the EBIT magnet was typically about 10^{-10} mbar; the pressure decreases progressively as one goes into the volume enclosed by the 40 K, 16 K shields and the 4 K magnet body, but it cannot be measured directly. The total gas pressure at the center of the trap, in its 4 K enclosure, was estimated to be of the order of 5×10^{-11} Torr [18] for the LLNL-EBIT. Due to enhanced differential pumping in the case of the Heidelberg EBIT, an even lower value is expected. The gas injector was fed with natural argon (99.60% of ^{40}Ar, 0.34% of ^{36}Ar, and 0.06% of ^{38}Ar), and also with ^{36}Ar (99.7% of ^{36}Ar, 0.3% of ^{40}Ar) (for a total acquisition time of 960 min with this latter isotope). The two drift tubes located the closest to the trap region (DT#4 and DT#5) were used to trap ions axially by biasing them to 1500 V. Every 10, the trap content (trapped ions) was dumped by applying a HV pulse to the central drift tube for 100 ms. This prevented the accumulation of ions of heavy elements such as Ba or W, which evaporate from the cathode in only minute quantities but can nonetheless fill the trap after several minutes without this procedure.

III. DATA ANALYSIS

A. Fitting functions

Figures 3 and 4 show four examples of typical decay curves taken at different injection gas pressures. It is clearly

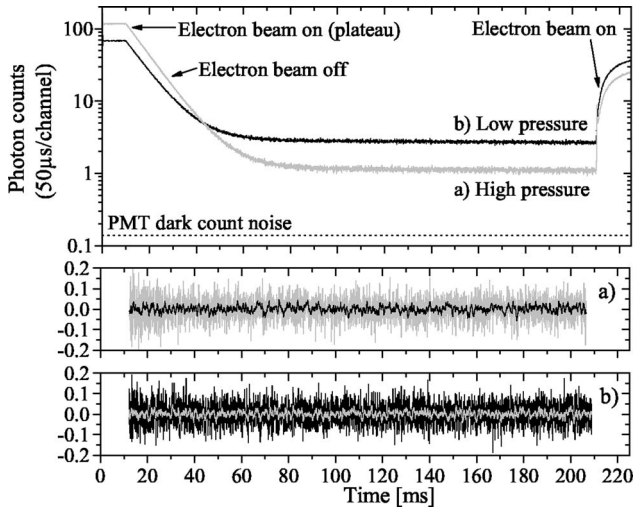

FIG. 3. Decay curves and their residuals (normalized by $\sqrt{N}$, where N is the number of counts in each channel) obtained during the first series of measurements at two different injection gas pressures for an electron beam turn-off time of 200 ms. The decay curves are normalized for a acquisition time of 60 s. We observed no correlations between the measured short decay times and the slowly decaying component, suggesting that it does not influence our lifetime measurement. Hence the slow component is attributed to excitation of Ar XIV ions to the $2p\ ^2P^o_{3/2}$ metastable level by low-energy electrons (see text for details).

observed that higher pressure results in an increase of intensity which is reflected by the heights of the plateaus observed 10 ms before turning off the electron beam. The measured decay curves were found to show two distinguishable components: a short 10 ms component attributed to the decay of the $2p\ ^2P^o_{3/2}$ metastable level and a slow component contribution of an apparent 1-s decay time. Both decay times were extracted by least-squares fitting (statistical weighting) (Microcal ORIGIN™) the observed decay curves with a two-exponential function including a correction to take into account the measured average dead time of the DAQS given by

$$N_{\text{obs}} = N_{\text{true}}\left(1 + \frac{N_{\text{obs}} t_{\text{dead}}}{t_{\text{acq}}}\right)^{-1}, \tag{1}$$

where N_{obs} is the number of photons observed (or counted) in each channel (50 and 111.11 μs long for the first and second series of measurements, respectively) at a time interval t, t_{acq} is the total acquisition time per channel, and N_{true} is the true photon count.

The experimentally recorded curve can be described very well by a sum of two exponential functions and a constant offset:

$$N_{\text{true}_c} = a_1 e^{-t/t_1} + a_2 e^{-t/t_2} + y_o, \tag{2}$$

where the free parameters a_1 and a_2 represent the initial intensities of the fast and slow components, and t_1, t_2 their respective decay times. The measured PMT dark count rate was y_o.

Attempts to use any other fit functions including three or more exponentials or $1/t$ components failed to yield a satisfactory representation of the data, showing large values of χ^2 and decreasing values of R^2. In some cases, these trial functions did not converge at all, i.e., by yielding errors larger than the fitted values. Also, a Fourier transform of the residuals did not show any unexpected patterns. The χ^2 and R^2 obtained were on average 1.15 and 0.999, respectively. In order to avoid possible systematic effects due to instabilities during the turning off of the electron beam, the fitting procedure was started 2 ms after that time. As will be shown in Sec. III B 7, a standard tail-fit analysis revealed fluctuations mostly within the statistical uncertainties of each of the individual lifetime measurements.

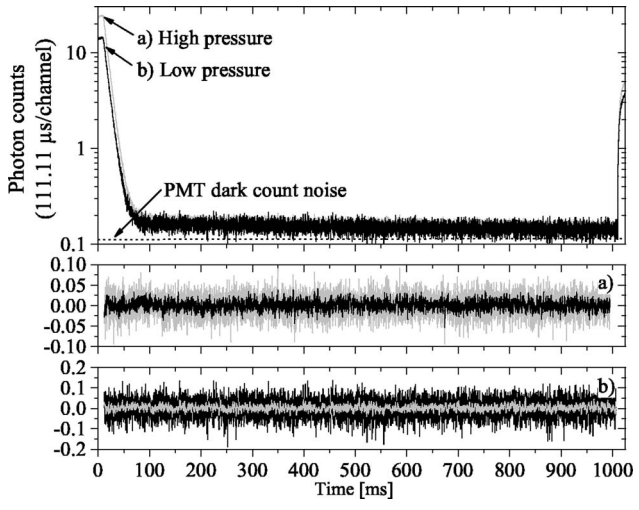

FIG. 4. Decay curves and their residuals obtained during the second series of measurements at two different injection gas pressures for an electron beam turn-off time of 1 s. For that second series we realigned the electron gun resulting in a weaker slow component due to less trapped electrons (see text).

B. Systematic effects

1. Radial and axial ion losses

After turning off the electron beam, the Ar XIV ion population might have been altered significantly due to ions leaving the trap along the axial and radial directions. Ions trapped by the potential wells created by the drift tube potential and the magnetic field could collide with each other, and, whereas some of them could lose kinetic energy, some others could gain sufficient energy to overcome these potential barriers and escape the trap (evaporative cooling). This resulted in a cooling of the ion ensemble but also in a slow loss of Ar XIV ions, embedded with the decay of the metastable level, which could have led to a significant apparent shortening of its lifetime.

To investigate the effect of axial ion losses, we measured decay curves at different drift tube potentials increasing from 100 to 1500 V in the first series of measurements and from 0 to 2500 V in the second series. Figures 5(a)–5(c), show the variations of the short decay time (t_1) and the decay rate $(1/t_2)$ of the slow component as a function of the drift tube potential for both series of measurements. As seen in Figs. 5(a) and 5(b), the short decay time increased with the trap-

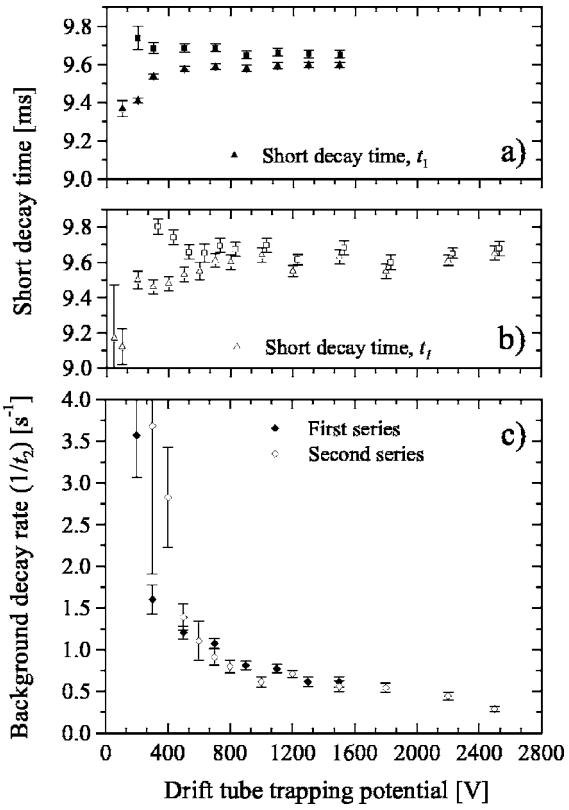

FIG. 5. Variations of the short decay times of the decay curves for the a) first and b) second series of measurements, and also c) the decay rate of the slow component ($1/t_2$), for both series, as a function of the drift tube trapping potential. The apparent constant value of the short decay times for trapping potentials higher than about 500 V agrees with a theoretical estimate of the axial ion escape rate indicating negligible ion losses within a ms time scale. The squares result from a hypothetical correction by the decay rate of the slow components ($1/t_1$-$1/t_2$).

ping potential raising from 0 to about 500 V and then reached an apparent constant value at trapping potentials from 500 to 2500 V. This indicates that, for drift tube potentials of a few kVs, the ion escape rate out of the trap was negligible in comparison to the short decay time. The slow component observed in the spectra might be an indication of ion losses. As seen in Fig. 5(c), its decay rate constantly decreases while its intensity grows (see Ref. [19]) as the trapping potential is raised. However, the short decay time appears to be independent of this component. As we will discuss in detail in Sec.IV B, we have strong evidence that the slow component was produced through the trapped Ar XIV ions interacting with a slowly decaying population of low-energy electrons trapped in the EBIT, which may have coexisted in the same region of space with the ions after turning off the electron beam, thus resulting in a reexcitation of Ar XIV ions to the metastable level.

The actual rate of axial ion losses can be estimated theoretically by assuming that the ions in the trap had a Maxwellian energy distribution and only those having a kinetic energy higher than the drift tube trapping potential could escape [20,21]. The number of ions $\frac{d}{dt}N_{esc_i}$ leaving the trap per unit time can be expressed as

$$\frac{d}{dt}N_{esc_i} = -N_i\left[\frac{3}{\sqrt{2}}\nu_{ij}\left(\frac{e^{-\omega_i}}{\omega_i} - \sqrt{\omega_i}[\mathrm{erf}(\omega_i) - 1]\right)\right], \quad (3)$$

where

$$\omega_i = \frac{q_i eV}{k_B T_i}, \quad (4)$$

N_i is the total number of ions in the charge state q_i in the trap, e the elementary charge, V the (axial) trapping potential, k_B the Boltzmann constant, and T_i the temperature of the ions in charge state i (in K). The Maxwellian-averaged ion-ion Coulomb collision rate ν_{ij} for ions in charge state i with those in charge state j, both having the same mass M_i, can be expressed, following [22], as

$$\nu_{ij} = \sum_j \frac{4n_j\sqrt{2\pi}}{3\sqrt{M_i}(4\pi\epsilon_\circ)^2}\frac{q_i^2 q_j^2 e^4}{(k_B T_j)^{3/2}}\ln\Lambda_{ij}, \quad (5)$$

where ϵ_o represents the vacuum permittivity, n_j the number density of ions in charge state j, and T_j their temperature. $\ln\Lambda_{ij}$ is the Coulomb logarithm for ion-ion collisions, which normally takes values between 10 and 20 [20,23]. By assuming that all the ions in the trap were Ar XIV, its value was estimated to be $\ln\Lambda_{ij} \approx 19$ for our experimental conditions.

The term between brackets in Eq. (3) represents the axial ion escape rate. From Eq. (4), one can see that this rate depends exponentially on the ratio ω_i of the potential well (drift tube potential times ionic charge state) to the ion average kinetic energy given by the translational temperature. This ratio basically indicates what fraction of the ions is on average free to escape.

The temperature of the Ar XIV ions in the trap was extracted from the Doppler width of the forbidden line. To measure it we used the optical spectrometer described in Refs. [3,4], and kept the EBIT at the same experimental conditions as in the decay curve measurements. By deconvoluting the six unresolved Zeeman components of the $M1$ transition using a fitting function including six Gaussian distributions and taking into account the spectrometer resolving power, we deduced an ion temperature of approximately $T_i = 350\ \mathrm{eV}/k_B$. For an ion charge of $q = 13$ and an applied potential of $V = 1500$ V, which result in a trapping potential of 19.5 keV, the ratio ω_i is approximately 50. At this high value of ω_i, the calculated axial escape rate is of the order of 10^{-30} s, and thus absolutely negligible relative to the ms lifetime. Axial losses are therefore excluded under these conditions.

This conclusion can be more clearly illustrated by comparing the theoretical and experimental escape rates both together obtained for various trapping potentials. The experimental escape rates can simply be obtained by subtracting the reciprocal of the constant value of 9.57 ms measured for high drift tube potentials [see Figs. 5(a) and 5(b)] from the reciprocal of the measured short decay times obtained for various trapping potentials. As seen in Fig. 6 for the second series, the theoretical and experimental escape rates appear to be in good agreement for high trapping potentials. However, there is disagreement for trapping potentials lower than about 200 V, where the theoretical escape rate seems to

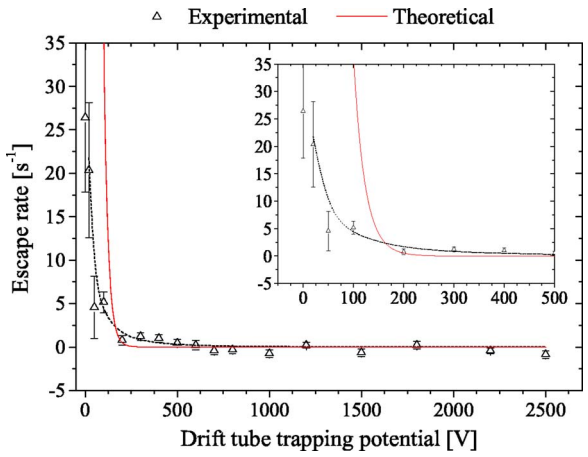

FIG. 6. (Color online) Theoretical and experimental escape rates for various trapping potentials. The experimental rates were obtained from the relation $(1/t_1\text{-}1/\tau)$, where τ was set equal to 9.57 ms. The disagreement observed between theory and experiment for low drift tube potentials can be explained by an overestimate of the ion temperature for low trapping potentials (see text) [the dashed line is only to guide the eye and is a fit of a $\exp-\omega_i/\omega_i$ function as Eq. (3)].

overestimate the experimental escape rate. Nevertheless, this large discrepancy can be explained by the fact that in the calculations of the theoretical rates we assumed an ion temperature of $T_i=350$ eV/k_B, which could not be a realistic temperature for such low trapping potentials.

In addition to ion losses in the axial direction, ions could also escape the trap in the radial direction due to transverse cross-field diffusion. Cross-field diffusion was treated in detail in Ref. [24]. Basically, in a homogeneous magnetic field, charged particles gyrate about a magnetic field line due to the $\boldsymbol{v}\times\boldsymbol{B}$ Lorentz force and thus remain radially trapped in a region of space defined by their gyration radius ($\sim$200 μm for Ar XIV ions at $T_i=350$ eV/k_B) until they experience a momentum changing collision. Collisions with charged particles as well as with neutral atoms let trapped particles drift in a random-walk towards regions of lower density. However, due to momentum conservation, ion-ion collisions lead to only weak diffusion. In collisions of particles with the same mass and charge, although the axes of gyration (guiding centers) can drift in opposite directions, the center-of-gravity of these axes does not significantly drift. The main concern here was therefore the possible drifts caused by collisions with neutral atoms. However, collisions with neutral atoms were negligible in this respect since for an Ar atomic diameter of about 340 pm [25] and a neutral number density of less than $\leqslant 10^6$ cm^{-3}, its rate was estimated to be less than 10^{-2} s^{-1}, insufficient to affect our measurements.

2. Charge-exchange ion losses

A particularly dangerous possible cause of changes in the charge state balance in the EBIT is the mechanism of charge exchange where HCIs capture electrons from neutral atomic or molecular species of the residual gas. This recombination can, on the one hand, result in the loss of metastable Ar XIV ions but, on the other hand, also increase their abundance if ions in higher charge states are present and recombine producing Ar XIV. Under such circumstances, and if charge exchange is significant due to a high neutral number density, a single-exponential function could not isolate contributions from various repopulation mechanisms and could yield essentially incorrect results. In order to quantify these additional contributions, one might be tempted to use a multiexponential function, but the results would also be incorrect. These uncertainties can be minimized by making sure that the neutral number density is reduced to a level at which no charge exchange takes place on the time scale of the lifetime under study. An additional cautionary measure is to avoid the production of ions in higher charge states. In the present experiment, the electron beam energy chosen ensured that no charge states higher than Ar XIV were present in the center of the trap. Hence charge exchange could only make the measured lifetimes shorter than the natural lifetime.

The above-mentioned gas injector brought the number density of neutral gas at the trap center to an estimated 10^4-10^6 atoms cm^{-3}. Based on the Müller-Salzborn charge-exchange cross section for single electron capture [20,23,26], the charge-exchange ion loss rate was then lower than . Note, however, this value is an upper bound estimate. In addition to this theoretical estimate, charge-exchange losses were experimentally checked by measuring the short decay time at injector gas pressures one order of magnitude lower and higher than the typical value used for our measurements. When we increased the injection pressure by a factor of 10, the pressure in the EBIT magnet increased to approximately twice as much as usual. These results did not show any discernible changes of the short decay times, besides of those of statistical nature, indicating that the charge-exchange effect was smaller than the statistical uncertainty of about 0.2% (this is the statistical uncertainty, which does not taking into account the dead-time uncertainty), in agreement with the previous theoretical upper limit.

These measurements at different Ar injection gas pressures did not only test the effect of the partial pressure of Ar but also of the residual pressure (or base pressure). By opening and closing the injection chamber, we observed that the Ar partial pressure in the EBIT outermost volume (between the EBIT inner wall and the 40 K thermal shield) was typically about 15% of the total pressure, while, by increasing the pressure in the injection chamber by one order of magnitude, the Ar partial pressure raised to about 50% of the total pressure. Hence, because the Ar partial pressure surrounding the electron beam was then a dominant portion of the total pressure, our measurements at various injection pressures were effective in determining whether charge exchange from neutral Ar or any other species was significantly affecting our measurements.

Moreover following a procedure introduced by Beiersdorfer *et al.* *K*-shell x-ray spectra were taken with a high-purity Ge detector (IGLET) after turning off the electron beam to evaluate the ion loss rate by charge-exchange recombination. Charge exchange will generate x rays after relaxation of the exchanged electron from the high principal quantum number into which it is captured. All the EBIT parameters were kept constant, except the electron beam energy which was raised up to about 10 keV in order to efficiently produce H-like and

bare Ar ions, which yielded easily detectable $K\alpha$ and $Ly\alpha$ photons. The measured x-ray emission was essentially identical to the dark count rate of the IGLET detector, and did not show any time dependence. This observation is in agreement with the result of Beiersdorfer *et al.* [15], who showed that Kr^{36+}, when trapped in the magnetic trapping mode, could survive in an EBIT for at least 5 s. *Z*-scaling this time constant for $q=13$, based on the Müller-Salzborn formula [20,23,26], yields an Ar XIV survival time of 17 s, i.e., a charge-exchange ion loss rate of $0.06\ s^{-1}$ very similar to our previous theoretical estimate. Even though we cannot detect any effect due to charge-exchange recombination, a loss rate of $0.1\ s^{-1}$ is included as a systematic error in our final lifetime.

3. Escape out of the line of sight

After turning off the electron beam, the ion cloud expanded mostly in the radial direction due to the sudden absence of the electron beam forcing a rearrangement of the ion orbits which were then governed by the repulsive Coulomb force between the individual ions. As a result, a significant number of ions might have escaped out of the line-of-sight of the light collection system. In a previous experiment by Serpa *et al.* at the NIST-EBIT [16], a spectrometer equipped with a slit assembly and a PMT was used as an optical detection system to select a well-defined spectral line. In that experiment, optical demagnification of the ion cloud and an adjustable slit allowed an effective field of view as wide as 2 mm, which could make the lifetime measurements sensitive to a radial ion cloud expansion beyond this value. These investigators carried out a series of studies using different slit widths and center positions in order to assess the associated systematic errors that contributed to a 1-σ overall uncertainty of several percents. It is to mention that immediately after turning off the electron beam, they observed a steep falloff of the signal during the first few μs at the beginning of the decay curves, indicating sudden ion losses out of the field of view of the detection system (radial and axial).

Our optical detection system had a wide field of view and a large acceptance angle, due to the arrangement of the lenses close to the trap, the 10-mm width of the slotted apertures on the side of the drift tubes and the use of the large diameter light guide along with a large diameter PMT. Particularly, by looking at the image of the ion cloud produced by the lenses on a CCD camera, we could totally image the slotted apertures and, hence, our optical detection system had an effective field of view wider than 10 mm. Thus the light collection efficiency was essentially unaffected by an ion cloud expansion up to a few mm in diameter. As an example, for high trapping potentials, we did not observe any steep falloff at the beginning of the decay curves that was actually present for trapping potentials $\leqslant 500$ V.

4. Dump-induced losses

The periodic HV dump applied for 100 ms every 10 s was not synchronized with the electron beam turn-off sequence. The probability of such a dump occurring during the deexcitation period of the data taking cycle induces total ion losses at a predictable rate of about $10^{-2}\ s^{-1}$. This rate was about one order of magnitude lower than our uncertainty. Nevertheless, the short decay times and the slow-component decay times were corrected for such losses.

5. Cascade repopulation

Repopulation of the $2p\ ^2P^o_{3/2}$ metastable level from higher levels could, in principle, have introduced systematic errors in our individual lifetime measurements. However, based on atomic-structure calculations, cascade repopulation was estimated to be negligible over a ms time scale. The transition probabilities from the closest low-lying levels in boronlike ions, the $2l2l'2l''$ and $2l2l'3l''$; were calculated for some ions in that isoelectronic sequence in Refs. [27,28]. Numerical results were interpolated to the Ar XIV ion by using a *Z*-scaling procedure. We estimated that all these low-lying levels decayed through VUV transitions within a few μs and, thus, had no significant contribution to the short decay time after a very short waiting time (2 ms).

Repopulation by cascades starting from $2l2l'nl''$ high-lying or otherwise Rydberg levels might also have affected our measurements. The lifetimes of these levels can be estimated from a hydrogenic equation [29,30] for $n \geqslant 2$ and $l \neq 0$ where n and l are the principal and orbital quantum numbers, respectively, by the following formula:

$$\tau_n = \frac{3\tau_o n^3 (l+1/2)^2}{4Z_i^4}, \tag{6}$$

where $Z_i = q_i + 1$ is the effective nuclear charge, and τ_o is the lifetime of the state of interest in hydrogen (or a lifetime obtained in highly charged ions but scaled to $q=1$). Based on Eq. (6), the Rydberg levels having ms lifetimes that might have perturbed our measurements were those with $l \cong P, d, f$, and with the principal quantum numbers of $n \sim 1000$ as well as $l \cong n-3$, $n-2$, $n-1$, and $n \sim 100$. However, due to the coupling of high-l to low-l levels resulting from Stark-induced l-mixing [31] by the electric field produced by the electron beam, the drift tubes, and in ion-ion collisions, these latter decay to the ground state at a rate similar to that of the low-l Rydberg levels of identical principal quantum numbers, which have lifetimes of a few μs. Problematic would be the presence of low-l $n \sim 1000$ levels. However, their ionization potentials are of the order of 0.002 eV, and their barrier-suppression critical electric field is less than 100 V/m. They are field ionized in the fields produced by the voltages applied to the drift tubes, by the space charge of the ion cloud, or in ion-ion collisions.

The $1s^2 2s 2p^2\ ^4P_{3/2}$ excited level with a lifetime of at most 10 μs [0.1 μs in B-like Fe (nuclear charge $Z=26$)[27,28]] is the metastable level with the second longest lifetime in boronlike Ar XIV, and was therefore the most likely one to affect our measurements. It has a branching ratio to the $2p\ ^2P^o_{3/2}$ level of around 80%. Repopulation of the metastable level by this quartet level mostly occurred over the first few μs after turning off the electron beam. By starting the fitting procedure at 2 ms ($\sim$100 lifetimes) after that time we made sure that cascade repopulation from this level was essentially unsignificant. Indeed, our tail-fit analy-

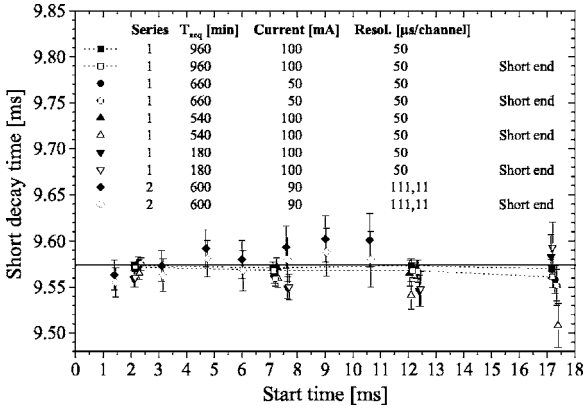

FIG. 7. Tail-fit analysis performed by varying the fitting interval from 2 ms to about 17 ms after turning off the electron beam and by shortening the end point by a factor of 2. The apparent trend in the decay time of the second series is statistically nonsignificant. The dotted lines emphasize the results obtained for the decay curve with the highest statistics.

sis presented in Sec. III B 7 did not show any effect of cascade repopulation.

6. Dependence on the electron beam current

Systematic effects related to the intensity of the electron beam during the ionization/excitation period were investigated by decreasing it from 100 to 60 and 50 mA during the first series of measurements. Some Ar XV ions were produced in these cases, because by reducing the electron beam current, the TSCP was reduced and, consequently, the effective electron beam energy increased. As an example, by decreasing the current by a factor of 2, the electron beam energy increased from 700 to 850 eV, which was then higher than the Ar XIV ionization potential. In spite of this fact, no variations of the short decay times within the experimental statistical uncertainty of less than 0.2% were observed. The intensity of the slow component, however, decreased by about a factor of 2.

7. Tail-fit analysis and correlation studies

To investigate systematic errors that might have occurred at the beginning of the decay curves caused by, for instance, cascade repopulation, the dead time, or an intensity dependence of the PMT detection efficiency, and also in order to test the validity of the fitting function, we performed a tail-fit analysis. Decay curves were fitted at various intervals, starting from 2 ms up to about 17 ms after turning off the electron beam and shortening the end by a factor of 2 (from 200 to 100 ms or from 1000 to 500 ms). The results are shown in Fig. 7. No unexpected trends and significant changes of the measured short decay times can be seen there. The positive slope observed for the decay curve obtained during the second series has no statistical significance because it is the result of low statistics and the long integration time per channels (111,11 μs per channel).

In addition to such a tail-fit analysis, we investigated possible correlations which might indicate systematic effects by

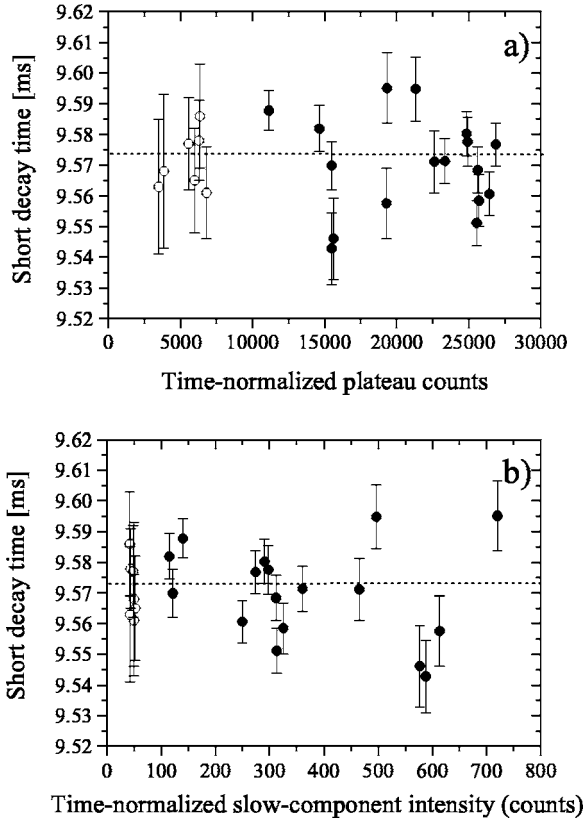

FIG. 8. Studies of possible correlations between the short decay time and (a) the time-normalized height of the plateau and (b) the time-normalized intensity of the slow component. Closed circles: first series of measurements, open circles: second series.

plotting the short decay time as a function of the time-normalized height of the plateau, the time-normalized intensity of the slow component, the plateau-normalized intensity of the slow component, as well as its decay time. These plots are shown in Figs. 8 and 9. Again, no apparent correlations can be discerned. The short decay time appears to be independent of these quantities and its variations are consistent with statistical fluctuations.

8. Dead time

After charge-exchange recombination, the dead time of our data acquisition system was the most important source of systematic errors. It was measured employing a digital oscilloscope (Tektronix, 500 MHz, 1GS/s) at various occasions and at different count rates (20 and 6 kHz) with the electron beam constantly on. The results obtained in all these independent measurements were in mutual agreement within their uncertainties. We obtained a mean value of 1.4(1) μs.

Due to pile-up effects, one might expect that the mean dead time might have slightly varied as a function of the signal count rate. However, the tail-fit analysis presented in Fig. 7 shows that our dead-time correction was not significantly affected by the different photon count rates, because by starting the fitting interval at various times after turning off the electron beam (i.e., various count rates) one observed variations which appear to be in agreement with statistical

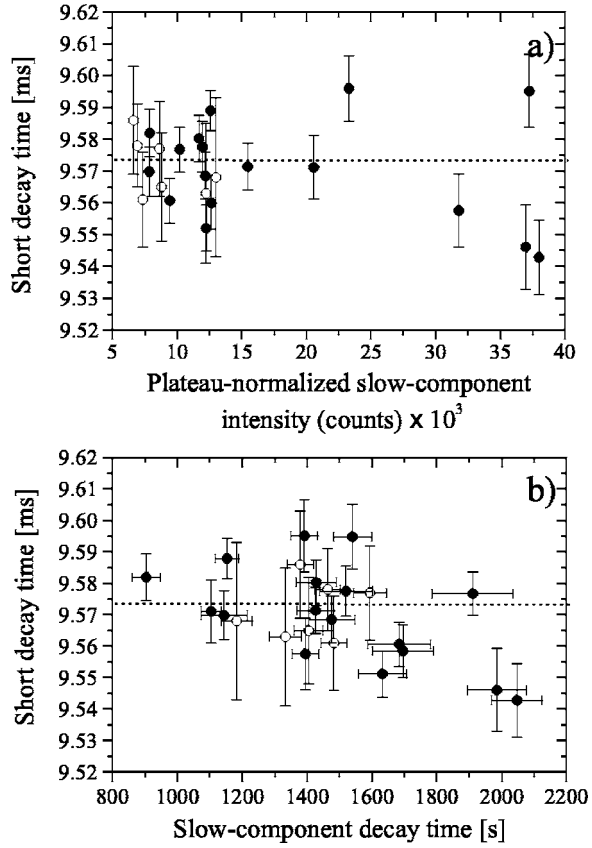

FIG. 9. Studies of possible correlations between the short decay time and (a) the plateau-normalized intensity of the slow component and (b) the slow component decay time. Closed circles: First series of measurements, open circles: second series.

fluctuations. In particular, the count rate at the plateau in the first and second series was different by about a factor of 3. Without the dead-time correction, the short decay times appeared longer by about 0.5% and 0.15%, respectively. Regarding the first series only, the exclusion of such a correction was clearly seen in the residual plots. In that case, when we left the dead time as a free parameter for the fit, the short decay times were reduced (on average) by about 0.15%. Despite all these differences, when we included the dead-time correction, we measured essentially the same short decay times for both series. Moreover, the validity of this correction was also investigated by plotting the short decay time as a function of the time-normalized height of the plateau, which is essentially a measure of the initial count rate when the electron beam was on. As seen in Fig. 8(a) for both series, the measured short decay times mostly varied within their errors bars, in agreement with statistical fluctuations.

IV. ORIGIN OF THE SLOW COMPONENT

A. Charge-exchange recombination of Ar XV ions

In previous experiments at the Lawrence Livermore National Laboratory (LLNL) EBIT, a background similar to our slow component was observed when increasing the electron beam to keV energies [32]. This background was attributed to charge-exchange recombination of ions of charge states higher than that under investigation. Hence the explanation for our unexpected slow component could be charge-exchange recombination of Ar XV ions because a certain amount (and higher charge states) might have been produced in the region of the drift tubes and constantly slipped into the trap when the electron beam was on [33].

However, if our slow component was mostly due to charge exchange of Ar XV ions, the measured decay rates shown in Fig. 5(c) as a function of the drift tube trapping potential should correspond to the loss rates of Ar XV ions in the trap. Essentially, these loss rates should be equal to those of Ar XIV ions. Coulomb collisions are more efficient for Ar XV ions since the ion-ion Coulomb collision rate is a function of q_i^2 [see Eq. (5)], however, such ions are more tightly bound to the trap than Ar XIV ions [see Eq. (4)] and hence the ratio between the Ar XV and Ar XIV axial loss rates is approximately equal to unity ($q_{\mathrm{Ar\ XV}}/q_{\mathrm{Ar\ XIV}}=1.1$) (assuming that both ions had essentially the same temperature in the trap). Similarly, the ratio of the charge-exchange rates of Ar XV and Ar XIV ions is also close to one since the Müller-Salzborn cross section [26] is proportional to $q_i^{1.2}$. Thus if the decay rate of the slow component was equal to the ion loss rate of Ar XIV, the difference between the decay rates of the fast and the slow components $[(1/t_1-1/t_2)^{-1}]$ measured for a given trapping potential should be constant as a function of the drift tube potential. However, as seen in Figs. 5(a) and 5(b), this is not what we observed. Instead, the hypothetically corrected short decay times increased for lower drift tube potentials (see Fig. 5 caption). This suggests that the decay rates of the slow component overestimated the true rates of ion losses in the trap, which we found negligible in Sec. III B 2. In addition, in Fig. 9, we observed no apparent correlation between the decay times of the fast and slow components, which should have both an inverse correlation if the slow-component decay time was an indication of ion losses. Therefore we do not find any indication that the slowly decaying component was caused by charge exchange.

B. Trapping of low-energy electrons

The slowly decaying component, even though it does not influence the determination of the lifetime of the metastable level within the given accuracy, remained a puzzling feature for a while. Let us summarize some of the observations. It is most pronounced at high trapping potentials, and its intensity grew with them. The decay time was between 1 and 2 s, much longer than the short decay time of 9.57 ms. Its lifetime increased with the drift tube potential but cannot be attributed to charge-exchange recombination since we observed no correlations with the measured short decay times. In addition, if the electron beam was not fully turned off, but a low current of, say, 1 mA was left on, the slow component disappeared (see Sec. IV B 9).

Eventually, this phenomenon was attributed to trapped electrons of an energy of less than $\approx$100 eV collisionally exciting Ar XIV ions to the metastable level (and also to a smaller extent to synchrotron as well as bremsstrahlung radiation produced by these electrons). After turning off the

electron beam, we have strong arguments to support the hypothesis that free electrons present in the trap region were trapped by the combined effects of the EBIT magnetic field, acting as a magnetic bottle, and the positive space charge potential of the ion cloud. In the following section we show that these assumptions are plausible and consistent with our observations.

These trapped electrons might have been those freed by electron-impact ionization of HCIs. However, we believe that they were the consequence of the alternating voltage applied to the focus electrode during switching-off the electron beam, which briefly defocused the beam before it completely went to zero. Electrons having lost their propagation direction along the drift tube assembly and the magnet axis during this process could have then been attracted towards the trap center by the drift tubes at high positive potential where a certain amount could have remained trapped by the EBIT magnetic bottle. This assumption is supported by the fact that the intensity increase of the slow component observed for increasingly high drift tube potentials was not proportional to the observed increase of the height of the plateau. Although, by increasing the drift tube potential from 100 to 1000 V, their height increased by about a factor of less than 2, the intensity of the slow component increased by as much as one order of magnitude (see Ref. [19]). This is explained by the fact that for increasingly high drift tube potentials, we were not only more effective in trapping ions but also attracting electrons coming from a defocused electron beam. If this hypothesis is true, one would expect that this source of systematic error would not be present in previous measurements that directly switched off the electron beam by reducing the anode voltage to zero, leaving the focus voltage constant (for instance, see Ref. [16]).

1. Magnetic bottle

The 8-T magnetic field was produced by two identical superconducting coils. In a perfect Helmholtz configuration the magnetic-field flux density has a single maximum located between the two coils. However, the HD-EBIT has only a "quasi-perfect" Helmholtz configuration with two maxima of about 8.3 T located 25 mm away from the center of the trap, which was at 8 T (see Fig. 1). This field configuration constitutes a so-called magnetic bottle which has, by itself, the capability of trapping electrons in the axial direction having an estimated pitch angle greater than about 76°[34] (neglecting plasma effects). The particular position of the field maxima just between the 40-mm long central drift tube assembly and the closest drift tubes might have prevented trapped electrons from falling into the deep positive potential of the nearby drift tubes.

2. Ion cloud space charge potential

In addition to the magnetic-bottle configuration, the ISCP also had the capability of confining low-energy electrons at the trap center. The ISCP can be estimated from the total space charge correction (TSCP) Φ_T, which can be obtained from the difference between the total electron beam energy E_{eff} and the applied potential difference between the cathode and the drift tube assembly E_{dt} [18,35]:

$$E_{eff} = E_{dt} + \Phi_T. \tag{7}$$

E_{eff} was obtained experimentally by sweeping E_{dt} near the ionization potential of Ar XIV and measuring the energy position where a maximum of the fluorescence signal was observed. At this position, E_{eff} is expected to be nearly equal to the Ar XIV ionization potential. For our experimental conditions, Φ_T was measured to be about −300 V.

The ESCP could not be measured. The ESCP Φ_e is a function of the beam energy E_e, current I_e, and radius r_e and can be described by the following equation [18,21,35]:

$$\Phi_e[\mathrm{V}] \approx \frac{30 I_e[\mathrm{A}]}{\sqrt{1 - \left(\frac{E_e[\mathrm{keV}]}{511} + 1\right)^{-2}}} \left(\ln\left(\frac{r_e}{r_{\mathrm{dt}}}\right)^2 - 1 \right). \tag{8}$$

A rigorous calculation of the electron beam radius with a nonlaminar electron beam of cylindrical shape and taking into account the thermal motion of the electrons using the Herrmann formula [36] yielded under our experimental conditions a value of ~25 μm. Hence one can estimate that Φ_e was about −550 V at the beam radius. The ISCP Φ_{ion} can simply be defined as

$$\Phi_{ion} = \Phi_T - \Phi_e. \tag{9}$$

Using this relation, we obtained Φ_{ion}=250 V, which is a value that is indeed sufficient to attract electrons trapped by the magnetic bottle towards the trap center.

3. Electron temperature and density

In order to excite Ar XIV ions to the metastable level, the electrons confined within the ion cloud must have a kinetic energy higher or equal to its excitation energy of about 2.8 eV (441.25 nm). The average kinetic energy of the ensemble of trapped electrons is essentially described through its temperature T_e. An estimate for T_e can be obtained, neglecting the effect of the magnetic field, from the ratio ω_e of the barrier potential to the electron temperature $\omega_e = e\Phi_{ion}/(k_B T_e)$ [see Eq. (4)]. The temperature of an ensemble of trapped particles in thermal equilibrium with a heat sink remains below the barrier potential, so that ω_e takes, typically, values between 2 and 10 [21]. Hence, for Φ_{ion}=250 V, one can expect that T_e=25–125 eV/k_B, which is indeed sufficient to excite ions to the metastable level.

In addition, knowing T_e, the density of trapped electrons can be estimated from the photon count rate N_s produced by the slow component, which can be described as

$$N_s = \frac{\varepsilon_{eff} N_i k n_e (1/\tau)}{1/\tau + 2kn_e}, \tag{10}$$

where N_i is the total number of trapped ions, estimated to be 5×10^7 from an independent measurement of ions extracted from the EBIT, k is the electron excitation/deexcitation rate coefficient, n_e is the electron number density, ε_{eff} is the total detection efficiency of about 8×10^{-5} (geometrical solid angle, transmission efficiency, and quantum efficiency), and τ is the lifetime of the metastable level. For an average T_e=25–125 eV/k_B≅75 eV and a Maxwellian-averaged rate coefficient, which we calculated

to be about 3×10^{-9}cm^3 s^{-1} (see Ref. [37] and equations therein), the electron number density was estimated to be 5×10^7 cm^{-3}. This density is 60 times less than the ion number density of about 3×10^9 cm^{-3}.

4. Radiative cooling and electron-ion thermal exchange

The previous estimate of the electron temperature did not include the effect of the 8-T magnetic field. In such a field, the trapped electrons can cool down by emission of synchrotron radiation and lose all their kinetic energy with a time constant of $\tau_s \sim 50$ ms. However, these electrons can also experience inelastic Coulomb collisions with HCIs and gain kinetic energy. A more realistic estimate of the electron and ion temperatures and their time evolution can be obtained from rate equations describing the electron-ion thermal exchange. Using the Spitzer equation [38] to calculate the Coulomb collision time constant for coexisting ions and electrons to reach thermal equilibrium such as

$$\tau_{eq} = \frac{3\cdot 2^{1/2}\pi^{3/2}\epsilon_o^2 M_i m_e k_B^{3/2}}{n_e q_i^2 e^4 \ln\Lambda_{ei}}\left(\frac{T_e}{m_e}+\frac{T_i}{M_i}\right)^{3/2}, \tag{11}$$

where $\ln\Lambda_{ei}$ is the Coulomb logarithm for electron-ion collisions:

$$\Lambda_{ei} = \frac{4\pi}{q_i e^2}(\epsilon_o k_B)^{3/2}\left(\frac{T_e}{n_e}\right)^{1/2}\left(T_e+\frac{T_i m_e}{M_i}+2\sqrt{\frac{m_e}{M_i}T_i T_e}\right), \tag{12}$$

the time dependence of T_i and T_e can be expressed by the following two rate equations:

$$\frac{d}{dt}T_i = -\frac{1}{\tau_{eq}}(T_i - T_e), \tag{13}$$

$$\frac{d}{dt}T_e = \frac{N_i}{N_e}\frac{1}{\tau_{eq}}(T_i - T_e) - \frac{1}{\tau_s}(T_e - T_0). \tag{14}$$

For a cryogenic environment of $T_0=4$ K, an ion temperature of $T_i=350$ eV/k_B, and the electron and ion number densities mentioned above, our simulations show (see Fig. 10) that for a density ratio of $N_i/N_e \approx 60$, since the ion-electron Coulomb collision rate was higher than the cooling rate, the cooling of the electrons by synchrotron radiation was compensated by thermalization with trapped HCIs. The larger HCI ensemble, which cools through synchrotron radiation at a much slower rate, acted as a thermal reservoir for the minority trapped electrons. In this way, the electrons could keep a nearly constant temperature of about 100 eV sufficient to excite Ar XIV ions for more than 1 s, in agreement with our observations. It is interesting to compare this ion-electron dynamics to a hypothetical case where $N_i/N_e \approx 0.1$, with HCIs being the minority. In this case, as seen in Fig. 10, the trapped ions are cooled down by the electrons and, as a result, the electron temperature falls below the 2.8 eV excitation threshold in less then 1 s.

5. Decay of the slow component

Our various experimental measurements taken under different experimental conditions show that the dynamics of the trapped electrons in the ion cloud and their dynamics with the ions are quite complex, and will remain the subject of future investigations [19].

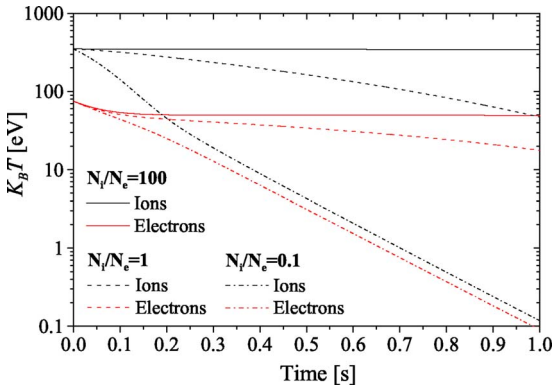

FIG. 10. (Color online) Theoretical temporal evolution of the temperature of coexisting highly charged Ar XIV ions and electrons in a plasma for ratios of the numbers of ions to electrons of $N_i/N_e=0.1$, 1, and 100. These temperatures were calculated for an ion cloud radius and length of 0.4 and 30 mm, respectively, and initial ion and electron temperatures of 350 and 75 eV, respectively. In the present experiment the N_i/N_e ratio was estimated to be about 60.

We believe that the decay of the slow component was caused by the dynamics of the electrons because, as seen in Figs. 8 and 9 we observed no correlations between the decay time of the slow component and its intensity as a function of the short decay time. In addition, as seen in Figs. 5 and 6 the escape rates of Ar XIV ions were found to be essentially constant and insignificant relative to the measured short decay times when we increased the drift tube potentials from 500 to 2500 V. At the same time, however, the decay rates of the slow component decreased and they could be fairly well described by a $\exp(-\omega_i/\omega_i)$ function as a function of the drift tube potential [see Eq. (3)]. Therefore we attribute the decay of the slow component mostly to trapped electrons leaving exponentially the ion cloud by evaporative cooling.

6. Cross-field diffusion by electron-ion impact

Ion losses induced by cross-field diffusion of Ar XIV ions due to collisions with trapped electrons were negligible. Considering a Maxwellian-averaged electron energy distribution, the Coulomb collision rate of an ion with electrons was estimated to be hundreds per second ($n_e=5\times10^7$ cm^{-3}). Hence we estimated based on a fully ionized plasma that the coefficient of cross-field diffusion was approximately 10^{-9} m^2 s^{-1}. For the dimension of our trap, this value yields a loss rate of the order of 10^{-6} s^{-1}, too low to affect our measurements.

7. Quenching by trapped electrons

After turning off the electron beam, the trapped electrons could have significantly reduced the population of ions in the metastable level by electron-impact deexcitation and excitation to upper-energy levels. For this reason, it is important to investigate the effect of quenching. Neglecting ion losses for

simplicity, the time evolution of the Ar XIV ion population in the metastable level $N_M(t)$ affected by electron impact can be basically described based on a two-level system [39]:

$$N_M(t) = \left(N_M(0) - \frac{N_i k n_e}{1/\tau + 2kn_e} \right) e^{-(1/\tau + 2kn_e)t} + \frac{N_i k n_e}{1/\tau + 2kn_e}, \tag{15}$$

where $N_M(0)$ is the initial number of ions in the metastable level before turning off the electron beam and τ is the natural lifetime. The first term represents essentially the decay of the metastable level, where the reciprocal of the argument $(1/\tau + 2kn_e)$ of the exponential function is the short decay time t_1, which, due to the presence of trapped electrons, is a reduced apparent lifetime that depends on the natural lifetime and the electron quenching rate $(2kn_e)$. The last term of Eq. (15) describes electron-impact excitation from the ground level to the metastable level producing a constant background. The situation is more complicated for a multilevel system. However, for the upper-energy levels that we are dealing with (μs lifetimes), basic simulations have shown that the effect of the low-energy electrons was essentially the same, i.e., they could only reduce the lifetime because they added other decay channels to the metastable level.

The quenching rate can be estimated from the intensity of the slow component by using Eq. (10). For a total number of ions in the trap of 5×10^7 and considering the decay curve having the slow component with the highest intensity, the quenching rate was estimated to be $\leqslant 0.3\ s^{-1}$, which is about 0.3% of the natural transition rate $(1/\tau)$. However, this estimate is only an upper limit to the quenching rate because it was based on a number of Ar XIV ions obtained from an independent measurement of ions extracted from the EBIT, which had at that time an axial trapping potential of about 300 V. The trapping potential used for the lifetime measurements was 1500 V, hence one can expect that the quenching rate was lower because the number of trapped ions was actually higher.

The actual importance of quenching in our measurements can be seen in Fig. 8, where the short decay time is plotted as a function of the intensity of the slow component. If quenching was significant, its influence should reveal itself in an inverse correlation between these two quantities. However, no correlation can be seen in this plot, indicating that quenching had an effect smaller than the experimental uncertainty. This will be investigated further in the next sections, coming to the same conclusion.

8. Electron-capture recombination

Losses by electron-ion recombination only affected our individual lifetime measurements within their error bars. The Maxwellian-averaged electron-ion recombination rate can be expressed as

$$R_r = n_e \int_0^\infty \sigma_r v_e(E) \left(\frac{1}{2\pi (k_B T_e)^3} \right)^{1/2} e^{-E/k_B T_e} dE, \tag{16}$$

where $v_e(E) = \sqrt{2E/m_e}$ and σ_r is a recombination cross section for a given electron energy E. For radiative recombination in the ground level of Ar XIV, this cross section can be obtained from Kim and Pratt [40] as

$$\sigma_r = \frac{16\pi}{3\sqrt{3}} \alpha \lambda_c^2 \frac{\zeta^2 I_H}{E} \ln\left[1 + \frac{\zeta^2 I_H}{E n_{eff}^2} \right], \tag{17}$$

where α is the fine-structure constant, λ_c is the electron Compton wavelength, I_H is the ionization potential of hydrogen, and $\zeta = (Z + q_i)/2$. n_{eff} is an effective quantum number equal to $n_{eff} = n_0 + (1 - W_{n_0}) - 0.3$, where n_0 is the principal quantum number of the valence shell and W_{n_0} is the ratio between the number of unoccupied states and the total number of states in the valence shell. For T_e of about 75 eV and an electron density of $5 \times 10^7\ cm^{-3}$, the electron-ion recombination rate was estimated to be of the order of $10^{-5}\ s^{-1}$. We also made an estimate based on the Seaton formula for hydrogenic ions [41], which yielded essentially the same result.

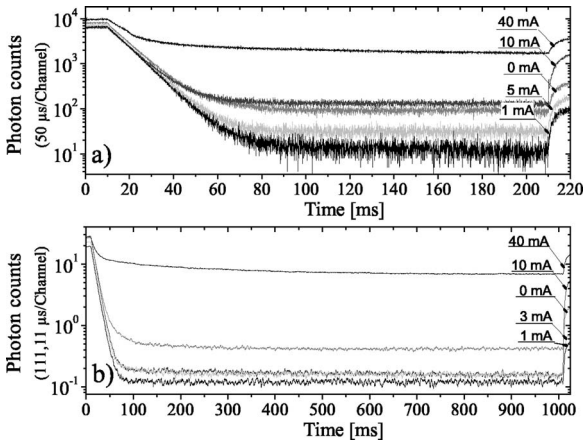

FIG. 11. Decay curves obtained by turning down the electron beam intensity. (a) First series and (b) second series of measurements. Each decay curve was taken for a total acquisition time of 1 h. The slow components obtained with no electron beam current (zero current, beam turned off) were higher than that obtained with an electron beam of less than about 5 mA (see text).

9. Electron beam turned off partially

An additional insight into the effect of quenching by trapped electrons can be obtained by comparing the fast and slow components to those obtained when the electron beam current is turned down to low intensities instead of being turned off completely. Decay curves obtained with low electron beam currents are shown in Fig. 11. Basically, when the electron beam was on above 20 mA, the short decay times were reduced as a consequence of the combined effects of quenching and depletion of the Ar XIV population by electron-impact ionization, because decreasing the electron beam current reduced the ESCP, increased the effective electron beam energy and, thus, enhanced ionization of Ar XIV.

By lowering the value from 20 to 0 mA, however, the short decay times became essentially longer due to increasingly lower quenching and depletion rates (see Fig. 12). An interesting phenomenon appeared at low currents. We observed that the signal measured with a beam current of 10

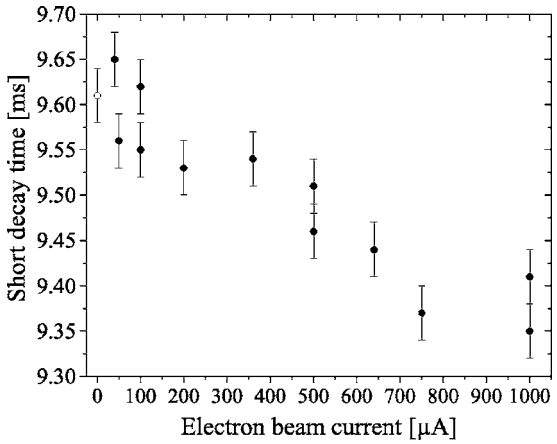

FIG. 12. Short decay times of decay curves taken as the electron beam current was left to a few μA (closed circles) and turned off totally (open circle). In the eventuality that quenching might have affected our lifetime measurements, these measurements taken as the electron beam was on indicate, nevertheless, a lower limit of 9.57 ms to the lifetime of the metastable level.

and 3 mA (first and second series, respectively) was identical in its slow component to that obtained when the electron beam was completely turned off. The slow component, however, disappeared completely if the beam was turned down to 1 mA. The depletion rate is the product of the electron-impact ionization cross section, which depends on the electron beam energy, and the electron beam current. By decreasing the beam current, the electron flux was reduced, but the beam energy increased and the Ar XIV ionization cross section also increased (before reaching its maximum value of about 2.3 keV). Because of this interplay between the beam current and ionization cross section, depletion was expected to reach its maximal rate around 50 mA. Hence the complete disappearance of the slow component around 1 mA and its revival when the electron beam current was turned off is interpreted as a consequence of Coulomb repulsion of low-energy trapped electrons by the ESCP of the energetic electrons of the low-current beams.

Moreover, and most importantly, the fact that the slow components observed when the electron beam was off were identical to the slow components observed when we turned down the electron beam to two different low-current values of 10 and 3 mA suggests that quenching did not affect our lifetime measurements as much as one could expect (0.3%). The intensities of the slow component at zero current obtained for both series were different by a factor of about 3, despite that the measured zero-current short decay times were essentially constant within their statistical uncertainties.

A further test was carried out. Figure 12 shows, for the second series only, a plot of the short decay time as a function of the beam current when the electron beam was switched to values lower than 1 mA. This figure shows that the short decay time increased for beam currents reduced from 1 mA to 50 μA, as expected (lower depletion and quenching rates), and approached for values below 50 μA the short decay time measured when the electron beam was off (in agreement with the y-intercept of the seemingly linear trend). Although this observation does not absolutely rule out quenching, it is nonetheless strongly supporting a lower limit of about 9.57 ms to the lifetime of the metastable level.

TABLE I. Table of error budget.

Systematic effect	Relative contribution (%)
Dead time	$\cong 0.06$
Charge-exchange losses	$\leqslant 0.1$
Statistics	$\cong 0.05$
Dump-induced losses	10^{-2}
Electron-ion recombination losses	$\sim 10^{-5}$
Radial ion losses	$\sim 10^{-2}$–10^{-6}
Axial ion losses	No
Cascade repopulation	No
Line-of-sight escape	No
Quenching	No

V. EXPERIMENTAL RESULT AND THEORY

A. Experimental result

After consideration of the various systematic effects discussed above, our final experimental result for the lifetime of the Ar XIV $2p\ ^2P^o_{3/2}$ level is $9.573(4)(^{+12}_{-5})$ (statistical)(systematic). This value was obtained from a weighted average of the measured short decay times of curves taken during various acquisition times ranging from 3 to 5 h, for a total acquisition time of about 116 h. The statistical error of ± 0.004 ms is the standard error of the mean of these measurements, while the systematic error of -0.005 and $+0.012$ ms is due to the dead time of the data acquisition system and the charge-exchange recombination loss rate, both added quadratically to set the upper uncertainty limit. As shown in Table I, where the error contributions are listed, these are the only significant systematic errors found. The contribution of the total systematic error to our experimental result is slightly different from that in our previous publication [8], where we did not include the effect of charge-exchange recombination because it actually could not be directly measured. However, we include this effect here to slightly enhance the confidence limit of our final error bar.

B. Theoretical $M1$ transition probabilities between fine-structure energy levels

The relativistic probability of a $M1$ transition from an initial state i to a final state f can be expressed as [42]

$$A_{if} = \frac{64\pi^4}{3h}\frac{1}{\lambda^3}\frac{S_{if}}{2J_i+1}, \tag{18}$$

where h is the Planck constant, c is the speed of light, λ is the wavelength of the transition (in vacuum), $2J_i+1$ is the multiplicity of the upper energy level, and S_{if} is the line strength of the $M1$ transition such as

$$S_{if} = \frac{9e^2}{4}\frac{\lambda^2}{(2\pi)^2}|\langle f\|j_1(2\pi r/\lambda)[\vec{r}\times\vec{\alpha}]/r\|i\rangle|^2. \quad (19)$$

Here $\vec{\alpha}$ is the vector of the Dirac matrices, and j_1 is the first-order spherical Bessel function. In the nonrelativistic *LS*-coupling approximation, the line strength $S_{if}^{\rm nr}$, which expresses the interaction of the electron magnetic moment with the field, can be written as the reduced matrix element of the total orbital and spin angular momentum operators, $\boldsymbol{L}$ and $\boldsymbol{S}$, respectively, and the electron g_e factor (field free theory), so that

$$S_{if}^{\rm nr} = \mu_{\rm B}^2|\langle f\|(\mathbf{L}+g_e\mathbf{S})\|i\rangle|^2, \quad (20)$$

where $\mu_{\rm B}=e\hbar/(2m_ec)$ is the Bohr magneton $[\hbar=h/(2\pi)]$. The nonrelativistic line strength $S_{if}^{\rm nr}$ is independent of the nuclear charge and can be expressed in terms of the quantum numbers L, S, and J. By taking the Landé electron g_e factor as equal to 2, the line strength of $M1$ transitions $(J_f=J_i-1)$ between levels of a given *LS* term can be determined from Racah algebra as equal to [43,44]

$$S_{if}^{\rm nr} = \frac{\mu_{\rm B}^2}{4J_i}(L+S+J_i+1)(L+S-J_i+1) \times(J_i+S-L)(J_i+L-S), \quad (21)$$

and, from Eq. (21), one can see that the nonrelativistic line strength of all $^2P^{\rm o}_{1/2}$-$^2P^{\rm o}_{3/2}$ transitions is a constant equal to $4/3\ \mu_{\rm B}^2$.

Based on Eq. (18), a theoretical transition probability is typically obtained by combining a theoretical transition wavelength to a theoretical line strength, which are both obtained independently from a self-consistent method. However, the error in the calculation of the transition probability introduced by the theoretical transition wavelength can be eliminated by combining an experimental transition wavelength to a theoretical transition line strength. By using this procedure, transition probabilities with an accuracy of less than 1% can be obtained for mid-Z ions from Eq. (21) because its relativistic corrections are basically proportional to powers of $(\alpha Z)^2$ and $1/Z$. In the leading order, the first relativistic term, which comes from the one-electron Dirac equation, is proportional to $(\alpha Z)^2$, while the second, which is the relativistic-interelectronic-interaction correction, is of the order of $(\alpha Z)^2/Z$. In Ref. [2] the probability of the $^2P^{\rm o}_{1/2}$-$^2P^{\rm o}_{3/2}$ transition in Ar XIV was calculated using the configuration-interaction method in the Dirac-Fock-Sturm basis (CIDFS) combined with perturbation theory in $1/Z$. From this calculation, the one-electron relativistic correction was derived to decrease the nonrelativistic transition probability by about 0.22%, while the relativistic-interelectronic-interaction correction (calculated by CIDFS including the contribution of the negative-continuum energy states) increased it by about 0.03%. The evaluated frequency-dependent part of the interelectronic-interaction correction added a contribution of about 5×10^{-4}%.

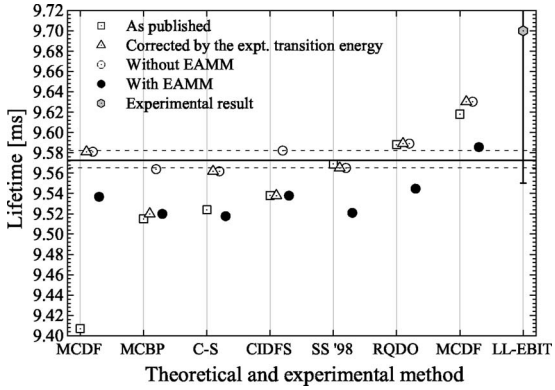

FIG. 13. Theoretical and experimental lifetimes [2,5,44–49].

The main QED correction to the line strength is that to the electron g_e factor. According to Landé and Dirac theories, g_e is equal to 2. However, one can add to this value a QED correction by including the electron anomalous magnetic factor κ_e such as

$$g_e = 2(1+\kappa_e). \quad (22)$$

Hence the main QED correction to the line strength can be calculated by adding κ_e to the nonrelativistic magnetic moment operator $\boldsymbol{\mu}^{\rm nr}$,

$$\boldsymbol{\mu}^{\rm nr} \rightarrow \boldsymbol{\mu}_{\rm a}^{\rm nr} = -\mu_{\rm B}[\boldsymbol{L}+2(1+\kappa_e)\boldsymbol{S}], \quad (23)$$

where $\boldsymbol{\mu}_{\rm a}^{\rm nr}$ is the magnetic moment of the bound electron including its so-called (electron) anomalous magnetic moment (EAMM). For $M1$ transitions between levels of the same *LS* term, this QED contribution to the line strength can be included by simply adding the multiplicative factor $(1+4\kappa_e)$ (see Ref. [2]) to the line strength such that Eq. (18) can be rewritten as

$$A_{if} = \frac{64\pi^4}{3h}\frac{1}{\lambda^3}(1+4\kappa_e)\frac{S_{if}}{2J_i+1}, \quad (24)$$

where $4\kappa_e$ $[\kappa_e\cong\alpha/(2\pi)]$ accounts for about 0.45% of the transition probability. This is larger than the relativistic contribution to the line strength of the Ar XIV $2p\ ^2P^{\rm o}_{1/2}$-$^2P^{\rm o}_{3/2}$ transition and is comparable to the 0.65% QED contribution to the transition probability caused by the 0.2% QED shift of the transition wavelength [3].

C. Comparison to theoretical calculations

Figure 13 compares our experimental result to some recently published theoretical lifetimes for the Ar XIV $2p\ ^2P^{\rm o}_{3/2}$ metastable level obtained using nonrelativistic (C-S [45], Breit-Pauli (MCBP [46]), and relativistic (Superstructure code (SS) [47], MCDF [48,49], CIDFS [2], and RQDO [44]) calculations.

For all these theoretical results, the lifetime of the metastable level was obtained from the reciprocal of the $^2P^{\rm o}_{1/2}$-$^2P^{\rm o}_{3/2}$ transition probability $(\tau\equiv1/A_{if})$, based on Eq. (18), by essentially dividing the line strength of the $M1$ transition by the cube of the transition wavelength which were both calculated independently. In order to obtain theoretical

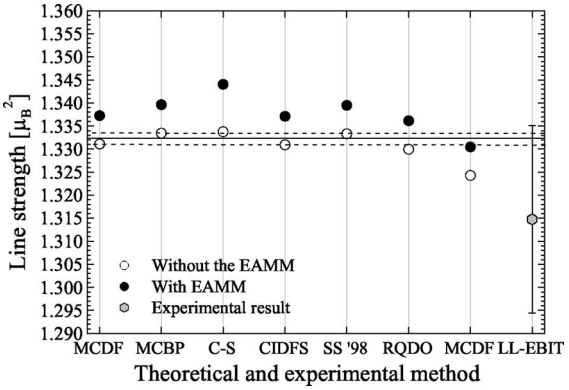

FIG. 14. Theoretical and experimental line strengths [2,5,44–49]. The line strength of the Ar XIV $2p\ ^2P^o_{1/2}$-$^2P^o_{3/2}$ transition that can be inferred from our final lifetime measurement is $1.3322(^{+9}_{-18})$, surprisingly in good agreement with the nonrelativistic line strength of 1.3333 [see Eq. (21)].

predictions of higher accuracies, we multiplied these theoretical transition probabilities by the cube of their theoretical transition wavelengths and then divided by the cube of the experimental transition wavelength [441.2559(1) nm in air [3] converted to 441.3799(1) nm in vacuum]. The resulting theoretical lifetimes corrected by the experimental transition wavelength are also presented in Fig. 13, where one can see that this correction brings most theoretical (corrected) lifetimes within our experimental uncertainty limit. The only exceptions are those by Krüger and Czyzak [50] and Bhatia *et al.* [51] whose published and corrected lifetimes are below 9.35 ms (not shown) and the MCDF predictions by Verhey *et al.* [49], who limited their MC treatment to the Coulomb complex, only. Figure 14 shows theoretical line strengths deduced based on Eq. (18).

Except for the calculations performed by Froese-Fischer (MCBP) [46] and us (CIDFS [2]), it should be noted that all the theoretical predictions, however, neglected the contribution of the EAMM to the electron g_e factor by taking $g_e=2$. Figure 13 also presents the theoretical lifetimes additionally corrected to include this EAMM contribution by dividing these lifetimes by $(1+4\kappa_e)$ [see Eq. (24)]. This procedure used to include this contribution agrees with the result obtained by Froese-Fischer (MCBP) [46] and relativistic CI calculations by Johnson [52] who obtained 9.578 and 9.534 ms without and with the EAMM. This EAMM correction brings all but Verhey *et al.* calculations, outside our uncertainty limit and the narrow scattering of the theoretical predictions seems to indicate that the lifetime of the metastable level is 9.53(1) ms.

Moreover, in Fig. 13, our measurement is compared to the latest experiment performed at the LLNL EBIT [5] of 9.70(15) ms, higher than our result by 0.84 standard deviations. It is to mention that the lifetime measurement technique developed at the LLNL EBIT was cross-checked and tested for consistency with the Heidelberg TSR storage ring [53]. Figure 13 does not include the two earlier measurements by Moehs and Church [6] and Serpa *et al.* [7] who measured, respectively, 9.12(18) and 8.7(5) ms, lower than our result by 2.5 and 1.7 standard deviations, respectively.

We cannot explain the discrepancy of our measurement with the theoretical trend. On the experimental side, one possible explanation might be unexpected systematic effects in lifetime measurements of long-lived metastable levels at EBITs and storage rings or in plasma environments. Recently, Beiersdorfer *et al.* [54] performed a precision lifetime measurement of the Al-like Fe XIV $3s^23p\ ^2P^o_{3/2}$ metastable level with an accuracy level of 0.57% and obtained a lifetime of 16.74(12) ms, while various calculations indicate 16.60 ms, on average. The most recent theoretical *ab initio* calculations yielded 16.61 ms [55]. However, the effect of the EAMM must also be included to these theoretical values since the lifetime of this level is affected by the same EAMM contribution as that of the Ar XIV $2p\ ^2P^o_{3/2}$ level. This correction brings down the theoretical trend by about 0.45% to approximately 16.54 ms, which is in disagreement with the LLNL measurement. A similar discrepancy is also seen in the recent lifetime measurement of the $3s^23p^5\ ^2P^o_{1/2}$ level in Cl-like Cu XIII at the TSR storage ring performed with an accuracy level of 0.2% [56]. Träbert *et al.* measured 2.390(5) ms in perfect agreement with three theoretical predictions of 2.39 ms, which do not include the EAMM. Adding this contribution to the theoretical results reduces the lifetime to 2.379 ms.

D. Influence of the magnetic field

The EBIT 8-T magnetic field might have modified the lifetime of the metastable level and this could explain the disagreement of our measurement with the theoretical predictions. Due to the Zeeman effect, the magnetic field removed the degeneracy of the m_J states of the ground and metastable levels and split them into sublevels of energies $E_i(B=0)+g_i\mu_B m_J B$, where $E_i(B=0)$ is the energy of the unperturbed ground or metastable levels i, g_i is the electron gyromagnetic ratio of a level i, and B is the magnetic field flux density. As a consequence, the energy levels were no longer defined by their total angular quantum numbers J (not conserved), but by the magnetic quantum numbers m_J. Hence, in a configuration-interaction framework, the energy of a given m_J state is then a function of all adjacent m_J states.

In the magnetic field, the $^2P^o_{3/2}$ level was split into four states $|m_J|=1/2$, $3/2$, while the $^2P^o_{1/2}$ ground level was split into two $|m_J|=1/2$ states. The $|m_J|=1/2$ states of the $^2P^o_{3/2}$ level were slightly perturbed by those of the ground level while the $|m_J|=3/2$ states remained basically unperturbed because the most adjacent $|m_J|=3/2$ states (configuration $2p^3$) were about 100 eV far above the $^2P^o_{3/2}$ level. Our configuration interaction Dirac-Fock Sturm calculations have shown that the changes in the line strengths induced by the 8-T magnetic field were too weak to be observed. For instance, the line strengths of the $|m_J|=3/2\rightarrow|m_J|=1/2$ and $|m_J|=1/2\rightarrow|m_J|=1/2$ transitions were modified by about 0.04% and 0.01%, respectively.

Additionally, the lifetimes of the states of the $^2P^o_{3/2}$ level were also perturbed by the magnetic field because of the dependence of transition probabilities on transition wavelengths [see Eq. (18)]. Our calculations have shown, however, that while the lifetimes of the $m_J=-3/2$ and

$m_J=+3/2$ states were increased and decreased, respectively, by about 0.13% (the center of gravity keeping a value of 9.538 ms), those of the $m_J=-1/2$ and $m_J=+1/2$ states were altered by less than 0.006%.

Therefore the effect of the magnetic field does not explain the discrepancy of our experimental value with the theoretical trend even if we take into account the position of maximum efficiency of our interference filter, which did not exactly match the transition wavelength under observation (442 nm against 441.25 nm). The variation of the lifetime introduced by this effect is negligible.

VI. CONCLUSION

We presented details of a lifetime measurement of the Ar XIV $1s^22s^22p\ ^2P^o_{3/2}$ metastable level performed at the Heidelberg EBIT [8]. The lifetime was determined to be $9.573(4)\binom{+12}{-5}$(stat)(syst) ms. Our experimental result is in disagreement with a trend of theoretical predictions of 9.53(1) ms, which were appropriately corrected for the experimental $2p\ ^2P^o_{1/2}$-$^2P^o_{3/2}$ transition wavelength and also for the contribution EAMM. We found other experimental lifetime measurements with an accuracy higher than 0.5% also in disagreement with theoretical results when the EAMM contribution is included. We discussed in detail various systematic effects which might have influenced our lifetime measurements, for instance, an unexpected slowly decaying component. We investigated the origin and influence of this component and found that the measured short decay times appeared to be independent of its intensity and decay time. Among all the systematic effects presented here, the two most likely ones which tend to increase the measured lifetime are (1) the dead time of the DAQS and (2) cascade repopulation (radiative trapping can also lead to longer lifetime measurements [57], however, this effect is negligible for the lifetime under investigation). Our analyses seem to indicate that these effects are still too small in comparison to the size of the discrepancy.

Finally, we performed very recently a third series of lifetime measurements of the Ar XIV $2p\ ^2P^o_{3/2}$ level by raising the drift tube trapping potential to high voltages at the same time as the electron beam was turned off. This procedure was used in order to perform our measurements on cold ions, only. We essentially obtained the same lifetime and the background still showed a slow decaying component. This technique was also used to measure the lifetime of the Fe XIV $3s^22p^2P^o_{3/2}$ level. Again, we essentially obtained the same result as Beiersdorfer *et al.* [54] result.

ACKNOWLEDGMENTS

We acknowledge support from HITRAP (Contract No. HPRI CT-2001-50036). V.M.S., I.I.T., and A.V. acknowledge support from RFBR (Grant No. 04-02-17574). We also thank U. D. Jentschura for discussions.

[1] V. M. Shabaev, Phys. Rep. **356**, 119 (2002).
[2] I. I. Tupitsyn, A. V. Volotka, D. A. Glazov, V. M. Shabaev, G. Plunien, J. R. Crespo López-Urrutia, A. Lapierre, and J. Ullrich, Phys. Rev. A (to be published).
[3] I. Draganić, J. R. Crespo López-Urrutia, R. DuBois, S. Fritzsche, V. M. Shabaev, R. S. Orts, I. I. Tupitsyn, Y. Zou, and J. Ullrich, Phys. Rev. Lett. **91**, 183001 (2003).
[4] R. Soria Orts, PhD thesis, Johann Wolfgang Goethe University of Frankfurt Am Main, Germany, 2006.
[5] E. Träbert, P. Beiersdorfer, S. B. Utter, G. V. Brown, H. Chen, C. L. Harris, P. A. Neill, D. W. Savin, and A. J. Smith, Astrophys. J. **541**, 506 (2000).
[6] D. P. Moehs and D. A. Church, Phys. Rev. A **58**, 1111 (1998).
[7] F. G. Serpa, J. D. Gillaspy, and E. Träbert, J. Phys. B **31**, 3345 (1998).
[8] A. Lapierre, U. D. Jentschura, J. R. Crespo López-Urrutia, J. Braun, G. Brenner, H. Bruhns, D. Fischer, A. J. González Martínez, Z. Harman, W. R. Johnson, C. Keitel, V. Mironov, C. J. Osborne, G. Sikler, R. Soria Orts, V. Shavaev, H. Tawara, I. I. Tupitsyn, J. Ullrich, and A. Volotka, Phys. Rev. Lett. **95**, 183001 (2005).
[9] J. R. Crespo López-Urrutia, B. Bapat, I. Draganić, A. Werdich, and J. Ullrich, Phys. Scr., T **92**, 110 (2001); J. R. Crespo López-Urrutia, B. Bapat, I. Draganić, B. Feuerstein, D. Fischer, H. Lörch, R. Moshammer, J. Ullrich, R. Dubois, and Y. Zou, Hyperfine Interact. **146/147**, 109 (2003).
[10] P. Beiersdorfer, B. Beck, S. Elliott, and L. Schweikhard, Rapid Commun. Mass Spectrom. **8**, 141 (1994).
[11] L. Schweikhard, J. Ziegler, P. Beiersdorfer, B. Beck, St. Becker, and S. Elliott, Rev. Sci. Instrum. **66**, 448 (1995).
[12] P. Beiersdorfer, St. Becker, B. Beck, S. Elliott, K. Widmann, and L. Schweikhard, Nucl. Instrum. Methods Phys. Res. B **98**, 558 (1995).
[13] J. D. Gillaspy, Phys. Scr., T **65**, 168 (1996).
[14] P. Beiersdorfer, B. Beck, St. Becker, and L. Schweikhard, Int. J. Mass Spectrom. Ion Process. **157**, 149 (1996).
[15] P. Beiersdorfer, L. Schweikhard, J. R. Crespo López-Urrutia, and K. Widmann, Rev. Sci. Instrum. **67**, 3818 (1996).
[16] F. G. Serpa, C. A. Morgan, E. S. Meyer, J. D. Gillaspy, E. Träbert, D. A. Church, and E. Takács, Phys. Rev. A **55**, 4196 (1997).
[17] Physics Laboratory, Physical Reference Data, Atomic database of the National Institute of Standard and Technology (http://physics.nist.gov/PhysRefData/ASD/index.html).
[18] K. Widman, Ph.D. thesis, University of Graz, Austria, 1998.
[19] A. Lapierre, J. R. Crespo López-Urrutia, J. Braun, G. Brenner, H. Bruhns, D. Fischer, A. J. González Martínez, V. Mironov, C. J. Osborne, G. Sikler, R. Soria Orts, H. Tawara, Y. Yamazaki, and J. Ullrich, in *Do Electrons and Ions Coexist in an Electron Beam Ion Trap (EBIT)?, Physics with Ultra-Low Anti-proton beams, Wako, Japan*, AIP Conf. Proc. No. 793 (AIP, Mclville, NY, 2005). p. 361.
[20] B. M. Penetrante, J. N. Bardsley, D. DeWitt, M. Clark, and D. Schneider, Phys. Rev. A **43**, 4861 (1991).

[21] F. J. Currell, *Electron Beam Ion Traps and Their Use in the Study of Highly Charged Ions, The Physics of Multiply and Highly Charged Ions*, edited by F. J. Currell(Kluwer Academic, Dordrecht, 2003), Vol. 1, pp. 39–75.
[22] J. D. Callen, *Fundamentals of Plasma Physics* (to be published).
[23] I. V. Kalagin, D. Küchler, V. P. Ovsyannikov, and G. Zschornarck, Plasma Sources Sci. Technol. **7**, 441 (1998).
[24] F. F. Chen, *Introduction to Plasma Physics and Controlled Fusion* (Plenum Press, New York, 1984).
[25] J. O. Hirschfelder, C. F. Curtiss, and R. B. Bird, *Molecular Theory of Gases and Liquids* (Wiley, New York, 1954).
[26] A. Müller and E. Salzborn, Phys. Lett. **62A**, 1391 (1977).
[27] M. S. Safronova, W. R. Johnson, and U. I. Safronova, Phys. Rev. A **54**, 2850 (1996).
[28] U. I. Safronova, W. R. Johnson, and A. E. Livingston, Phys. Rev. A **60**, 996 (1999).
[29] H. F. Beyer and V. P. Shevelko, *Introduction to the Physics of Highly Charged Ions, Series in Atomic and Molecular Physics* (Institute of Physics Publishing, Bristol, 2003).
[30] H. Marxer and L. Spruch, Phys. Rev. A **43**, 1268 (1991).
[31] M. A. Gearba, R. A. Komara, S. R. Lundeen, C. W. Fehrenbach, and B. D. DePaola, Phys. Rev. A **71**, 013424 (2005).
[32] E. Träbert, P. Beiersdorfer, G. V. Brown, A. J. Smith, S. B. Utter, M. F. Gu, and D. W. Savin, Phys. Rev. A **60**, 2034 (1999).
[33] Based on a neutral number density of 10^6 cm^{-3}, and using the Müller-Salzborn charge-exchange cross section [26] for single electron capture, we estimated that 10^7, Ar XV ions, i.e., the same estimated amount of trapped Ar XIV ions, are necessary to match the heights of the backgrounds observed during our measurements.
[34] J. D. Jackson, *Classical electrodynamics* (Wiley, New York, 1975).
[35] A. J. González Martínez, Ph. D. thesis, Ruperto-Carola University of Heidelberg, Germany 2005.
[36] G. Herrmann, J. Appl. Phys. **27**, 127 (1958).
[37] H. L. Zhang, M. Graziani, and A. Pradhan, Astron. Astrophys. **283**, 319 (1994).
[38] L. Spitzer, *Physics of Fully Ionized Gases* (Interscience Publishers, New York, 1956).
[39] P. W. Miloni and J. H. Eberly, *Laser* (Wiley, New York, 1988).
[40] Y. S. Kim and R. H. Pratt, Phys. Rev. A **27**, 2913 (1983).
[41] M. J. Seaton, Mon. Not. R. Astron. Soc. **119**, 81 (1959).
[42] I. I. Sobelman, *Atomic Spectra and Radiative Transitions* (Springer, New York 1979).
[43] E. U. Condon and G. H. Shortley, *The Theory of Atomic Spectra* (Cambrige University Press, Combridge, England, 1964).
[44] E. Charro, S. López-Ferrero, and I. Martín, J. Phys. B **34**, 4243 (2001).
[45] B. Warner, Z. Astrophys. **69**, 399 (1968); calculations based on Condon & Shortley theory, Ref. [39].
[46] C. Froese Fischer, J. Phys. B **16**, 157 (1983).
[47] M. E. Gavalís, C. Mendoza, and C. J. Zeippen, Astron. Astrophys., Suppl. Ser. **131**, 499 (1998).
[48] K.-T. Cheng, Y.-K. Kim, and J. P. Desclaux, At. Data Nucl. Data Tables **24**, 111 (1979).
[49] T. R. Verhey, B. P. Das, and W. F. Perger, J. Phys. B **20**, 3639 (1987).
[50] T. K. Krueger and S. J. Czyzak, Astrophys. J. **144**, 1194 (1966).
[51] A. K. Bhatia, U. Feldman, and J. F. Seely, At. Data Nucl. Data Tables **35**, 319 (1986).
[52] W. R. Johnson (private communication).
[53] E. Träbert, P. Beiersdorfer, G. Gwinner, E. H. Pinnington, and A. Wolf, Phys. Rev. A **66**, 052507 (2002).
[54] P. Beiersdorfer, E. Träbert, and E. H. Pinnington, Astrophys. J. **587**, 836 (2003).
[55] M. J. Vilkas and Y. Ishikawa, Phys. Rev. A **68**, 012503 (2003).
[56] E. Träbert, G. Saathoff, and A. Wolf, J. Phys. B **37**, 945 (2004).
[57] P. Erman and G. Sundström, Phys. Rev. A **43**, 5790 (1991).